Mehdi Allagui[1, 2], Othman B.k Hasnaoui [1, 2], Jamel Belhadj[1, 2]

J. Electrical Systems 9-2 (2013): 179-190

Regular paper

Exploitation of pitch control to improve the integration of a direct drive wind turbine to the grid

Journal of Electrical Systems

The objective of this paper is to improve the integration of direct drive wind turbines to the grid using pitch control. The proposed control strategy offers the possibility to regulate active and reactive powers delivered to the grid according to the Transmission System Operators (T.S.O) Request. Firstly, the control algorithm of the generator side converter is developed. For this converter, an MPPT algorithm and a pitch angle controller were designed in order to maximize and limit the extracted wind power. Secondly, a control scheme for the grid side converter was proposed. The main objectives of this control scheme are to keep constant the DC-link voltage and to control the reactive power delivered to the grid. Finally, the wind system performances were evaluated in terms of accordance with the Grid Connection Requirements (G.C.R). Different scenarios were simulated to evaluate the behavior and the stability of the wind system during normal operation conditions, power degradation and during grid faults.

Keywords: Direct Drive Wind Turbine; PMSG, Pitch Control; MPPT; Vector Current Control; Phase Locked Loop; Grid Faults; LVRT; G.C.R.

1. Introduction

In the last decades, electrical energy production from wind source has been continuously increased in developed countries. Consequently, the large increase of wind power penetration in power systems has lead to many new challenges for wind industry. These challenge179s are mainly related to the compliance with the grid operator requirements (TSO or DSO) [1]. To achieve this target, the improvement of wind turbine control strategies becomes a very important challenge for manufactures.

In this context, this paper presents a control strategy for direct drive wind turbines in order to face the technical problems of integrating wind generators in power systems. The control algorithm of the full scale back-to-back converter is divided in two parts; the control of the generator side rectifier and the control of the grid side inverter. The rectifier is mainly used to control the generator torque with an MPPT algorithm in order to maximize the output power at low and medium wind speeds. In addition, a pitch control is used to limit the rotor speed and, as a result, the limitation of the generated power at high wind speeds. The inverter is mainly used to keep constant the voltage of the DC-Link capacitors. In addition, it allows controlling the active and reactive powers injected to the grid. Finally, the simulation section presents the performances of the whole control strategy under different grid conditions and takes into account the grid connection requirements.

The paper is organized as follows: The first section presents the developed model of the aerodynamic subsystem which includes the pitch actuator. The second section describes the modelling of the grid connection in the Point of Common Connection (PCC) and the Phase Locked Loop (PLL) method which is used for the synchronization with the grid voltage. In the last section, the power quality and the transient stability of the wind system during normal and disturbed operations were simulated and analysed.

Corresponding author :Prof. Dr. Eng. Jamel BELHADJ ESSTT, B.P N°56, Montfleuy 1008 Tunis, TUNISIA, E-mail : Jamel.Belhadj@esstt.rnu.tn
(1) University of Tunis El Manar, LSE-ENIT B.P 37 le Belvédère 1002 Tunis Tunisia
(2) University of Tunis, ESSTT-DGE, B.P 56 Montfleury 1008 Tunis Tunisia
mehdieep@yahoo.fr, Othmanbk.Hasnaoui@esstt.rnu.tn, Jamel.Belhadj@esstt.rnu.tn

2. Direct drive structure

The control system of the direct drive wind turbine is divided in two parts, the generator side control and the grid side control. With a multi-pole Permanent Magnet Synchronous Generator (PMSG), there is no need for an excitation system. It is possible to operate at low speed without gearbox. The generator is connected to the grid through a full scale back-to-back power converter [2-3]. The decoupling between the generator and the grid through power converters presents a very important solution to comply with the G.C.R [4]. The whole control strategy of the wind system is shown in Figure 1.

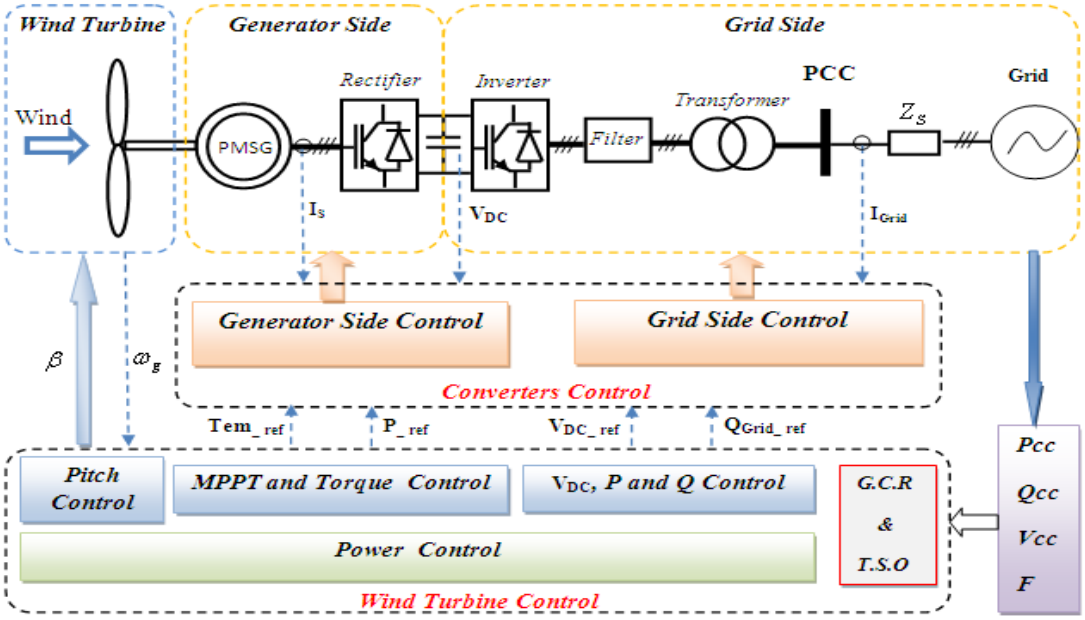

Fig. 1: General control scheme of Direct Drive wind turbine.

3. Power control system

3.1. MPPT Control

The mechanical power produced by a wind turbine is given by:

$$P_m = \frac{1}{2} C_p(\lambda, \beta).\rho.S.V_{wind}^3 \quad (1)$$

Where C_p is the power coefficient, β is the pitch angle in degree; ρ is the air density in (kg/m^3), S is the blades swept area (m²). V_{wind} is the wind speed (m/s) and λ is the tip-speed-ratio given by:

$$\lambda = \frac{R_{blade}.\Omega_g}{V_{wind}} \quad (2)$$

In equation (2), Ω_g is the generator angular speed and R_{blade} is the turbine radius. In order to produce the maximum wind power for each wind speed, the turbine should always operate at λ_{opt}. Figure 2 shows the mechanical power as a function of the rotor speed for different wind speeds. The parabolic curve gives the optimal regime related to optimal operating span.

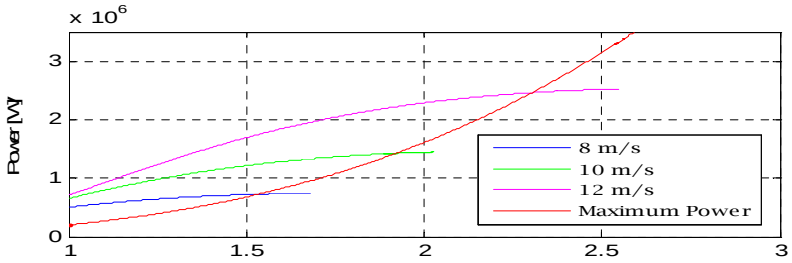

Fig. 2: The power-speed curve of the wind turbine.

The aerodynamic torque is given by the following expression:

$$T_m = \frac{P_m}{\Omega_g} = \frac{1}{2}\rho.\pi.R_{pal}^2.\frac{V_{wind}^3}{\Omega_g}.C_p(\lambda,\beta) \tag{3}$$

Power coefficient C_p can be approximated by analytical equations (4) and (5). Details and parameters of this model are given in [5]:

$$C_p(\lambda,\beta) = 0.22.(\frac{116}{\lambda_i} - 0.4\beta - 5).e^{\frac{-12.5}{\lambda_i}}) \tag{4}$$

Where:

$$\lambda_i = \frac{1}{(\frac{1}{\lambda + 0.08\beta} - \frac{0.035}{\beta^3 + 1})} \tag{5}$$

The aim of MPPT control is to set the power coefficient C_p to its maximal value: $C_p = C_{p\max}$ [6]. The torque reference is calculated through a set point from the shaft rotational speed based on relation (6) and (7):

$$T_{em\_opt} = \frac{P_{m\max}}{\omega_{gopt}} = K_{opt}.\Omega_{gopt}^2 \tag{6}$$

Where:

$$K_{opt} = \frac{1}{2}.\rho.\pi.R_{pal}^2.\left(\frac{R_{pal}}{\lambda_{opt}}\right)^3.C_{p\max} \tag{7}$$

3.2. Pitch Control

Pitch angle control is mainly used to limit the mechanical power during strong wind speed or to adapt power production according to the TSO requests. The aerodynamic behaviour of the wind turbine can be controlled actively by varying the turbine blade angle around their longitudinal axis [7]. In addition, in low and medium wind speed the pitch control is rarely actuated and only set to the optimum value, e.g. 0°. In high wind speeds, the pitch angle control effects to regulate the extracted wind power so that the design limits of the turbine will not be exceeded. Rotor speed, torque or power control can be taken to regulate the pitch angle [8]. In this paper, the power error criteria is used. The error between the reference power and the measured power at the output of the PMSG is sent to a PI controller to generate the reference value of the pitch angle β_{ref}. Mechanical power control and the complete model of the pitch system are shown respectively in Figure 3 and Figure 4.

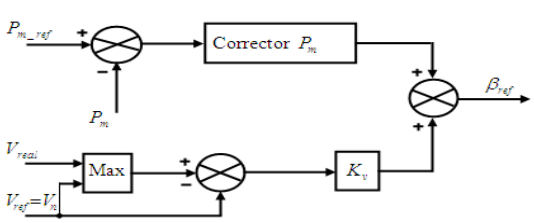

Fig. 3: Mechanical power control.

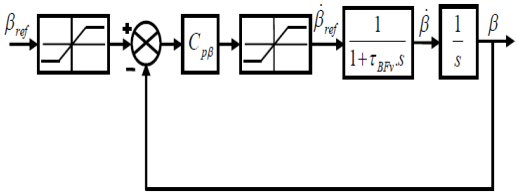

Fig. 4: Pitch angle controller block.

For the pitch angle controller, V_{ref} is the rated wind speed (12m/s). V_{real} is the actual wind speed. P_{m_ref} is the power reference value. P_m is the actual power. In the controller, "max" is used for selecting the maximum of the input to ensure that the pitch angle controller actuates only when the actual wind speed is greater than its rated value. This reference value is sent to the pitch actuator which can be electrical or hydraulic in order to turn the blades of the wind turbine. During normal operation, blade pitch adjustments with a rotational speed of approximately 5-10°/s are expected [9]. Here, the chosen pitch rate is 10°/s which avoids excessive loads during normal operation. Consequently, the complete model of the wind turbine by integrating the aerodynamic control is shown in Figure 5.

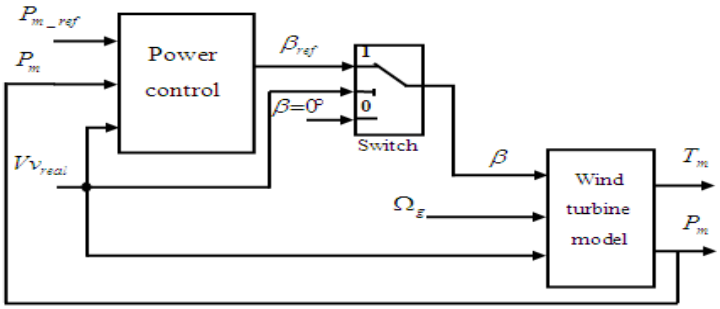

Fig. 5: Model of the wind turbine with a pitch angle control technique.

The switch used in this controller is activated by the wind speed V_{real} . When the wind speed is lower than the nominal value, the switch is connected to the position ' 0 '. It is connected to position '1' if the wind speed reaches or exceeds the nominal value. The following figures present simulation results of the torque control achieved with the MPPT algorithm and the pitch control. In order to test the operation of the grid side rectifier, the wind speed profile of Figure 6 is proposed.

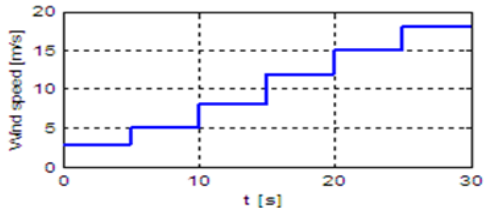

Fig. 6: Wind speed Vs time.

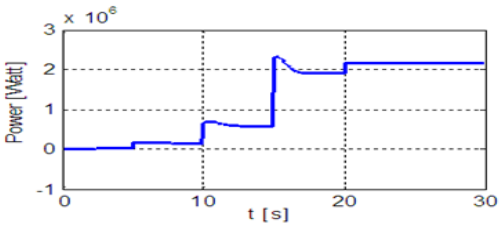

Fig. 7: Mechanical power Vs time.

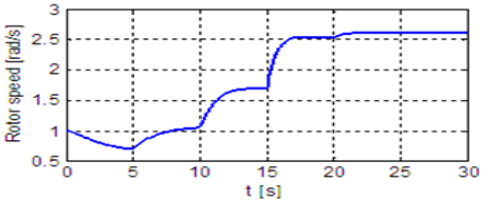

Fig. 8: Rotor speed Vs time.

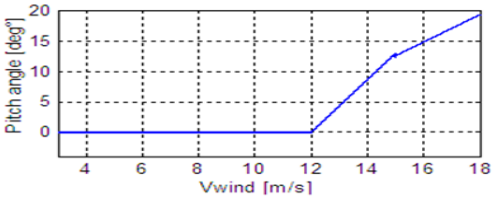

Fig. 9: Variation of the pitch angle Vs wind speed.

If the wind speed continues to rise, the generator output power remains constant (Figure 8). Figure 9 shows the curve of the pitch angle versus incoming wind speed. The aerodynamic model of the turbine allows the optimization of wind turbines exploitation. The typical power control regions of wind turbine results in Figure 10 is divided in two parts; the MPPT control operation and the pitch control operation. The turbine starts operating when the wind speed exceeds cut-in wind speed 5 m/s. At the set point of wind speed, the generating power reaches the rated wind power turbine 2MW.

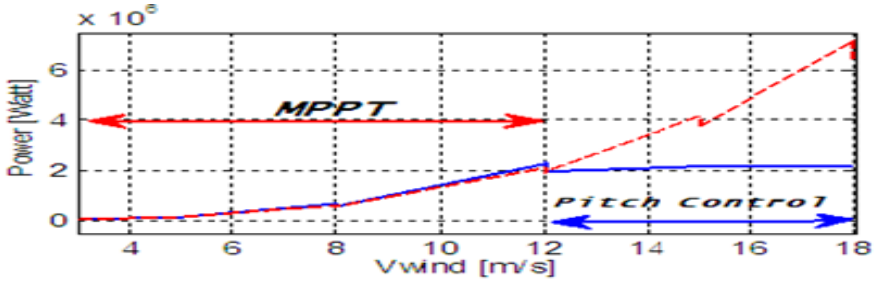

Fig. 10: Power curve Vs variable-speed pitch-controlled turbine

4. Modelling of the grid connection

The grid side inverter is connected to the grid through an LCL filter and a transformer (Figure 11).

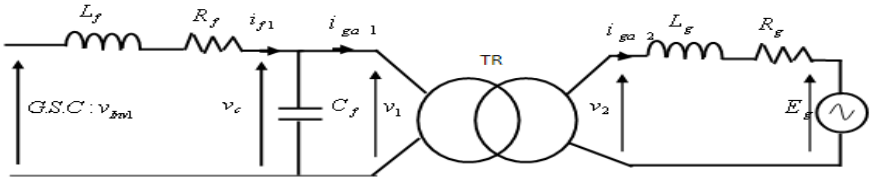

Fig. 11: Model of the connection to the grid.

This model is simplified by the following diagram brought back to the input of the transformer (Fig.12):

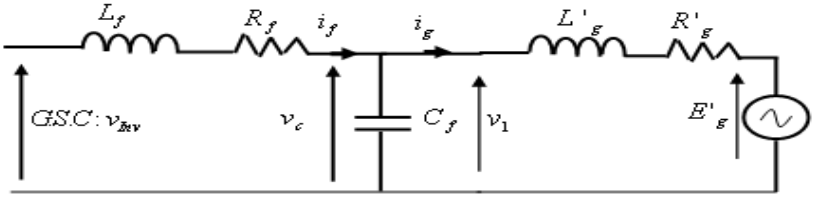

Fig. 12: Simplified diagram of the grid connection.

The model of this connection is described by the following equations:

$$V_{Inv} = R_f .i_f + L_f \frac{di_f}{dt} + V_1 \quad (8)$$

$$V_1 = R'_g .i_g + L'_g \frac{di_g}{dt} + E'_g \quad (9)$$

$$i_f = i_g + i_c \quad (10)$$

$$i_c = C_f \frac{dV_1}{dt} \quad (11)$$

From equations (8) and (9), relation (12) can be deduced :

$$V_{Inv} = R_f.i_g + R_f.C_f\frac{dV_1}{dt} + L_f\frac{di_g}{dt} + L_fC_f\frac{d^2V_1}{dt^2} + V_1 \quad (12)$$

In the reference frame (α,β), relation (12) can be written as follows:

$$\bar{V}_{Inv\_\alpha\beta} = R_f.\bar{i}_{g\alpha\beta} + R_f.C_f\frac{d\bar{V}_{1\alpha\beta}}{dt} + L_f\frac{d\bar{i}_{g\alpha\beta}}{dt} + L_fC_f\frac{d^2\bar{V}_{1\alpha\beta}}{dt^2} + \bar{V}_{1\alpha\beta} \quad (13)$$

Thus, the two components of V_{Inv} (V_{Inv_d} and V_{Inv_q}) in the Park reference frame are obtained:

$$V_{Inv\_d} = R_f i_{gd} + L_f(\frac{di_{gd}}{dt} - \omega_s i_{gq}) + R_fC_f(\frac{dV_{1d}}{dt} - \omega_s V_{1q}) + L_fC_f(\frac{d^2V_{1d}}{dt^2} - 2\omega_s\frac{dV_{1q}}{dt} - \omega_s^2V_{1d}) + V_{1d} \quad (14)$$

$$V_{Inv\_q} = R_f i_{gq} + L_f(\frac{di_{gq}}{dt} + \omega_s i_{gd}) + R_fC_f(\frac{dV_{1q}}{dt} + \omega_s V_{1d}) + L_fC_f(\frac{d^2V_{1q}}{dt^2} + 2\omega_s\frac{dV_{1d}}{dt} - \omega_s^2V_{1q}) + V_{1q} \quad (15)$$

The principle of grid currents control (I_{gq} and I_{gd}) is depicted on Figure 13:

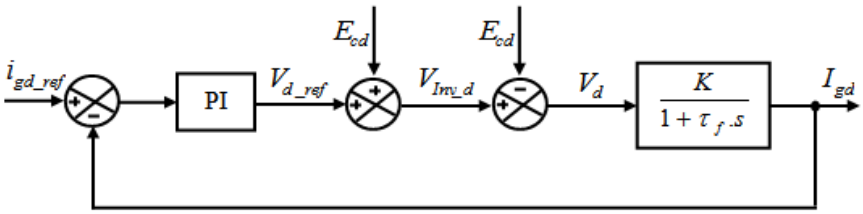

Fig. 13: Grid currents controller block diagram.

5. Grid voltage synchronization

In order to control active and reactive powers (P, Q) that flow to the grid, the control algorithm of the grid side converter must be synchronized with the grid voltage. To achieve this target, several techniques are used; the most used one is the phase locked loop "PLL" method [10]. This technique allows an accurate detection of the grid voltage angle θ_s. Figure 14 shows the PLL diagram.

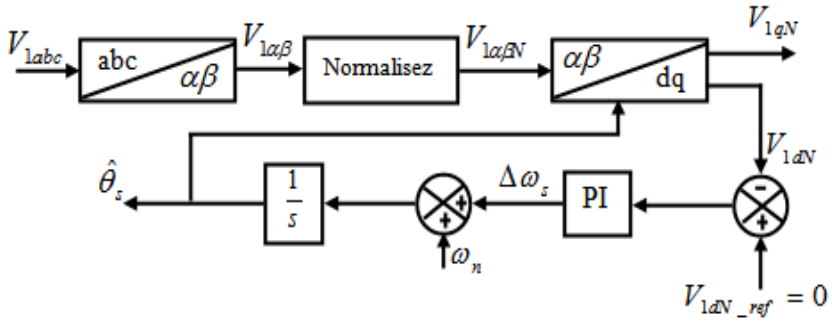

Fig. 13: PLL synchronization method.

The phase locked loop transfer function is given by:

$$H(s) = \frac{\hat{\theta}_s}{\theta_s} = \frac{K_p.s + K_I}{s^2 + K_p.s + K_I} \tag{16}$$

Equation (16) is comparable with the standard second order system with a zero:

$$H(s) = \frac{\hat{\theta}_s}{\theta_s} = \frac{2.\xi.\omega_0.s + \omega_0^2}{s^2 + 2.\xi.\omega_0.s + \omega_0^2} \tag{17}$$

With: $K_I = \omega_0^2 \; and \quad K_p = 2.\xi.\omega_0$

For this system, the cut-off frequency is chosen equal to the grid rated frequency $(\omega_n = \omega_0)$, with a damping ratio ξ equal to 0.7. Figure 15 shows the step response of the transfer function $H(s)$. It is a second order system with a zero. This zero introduces an overshoot of 20% with a 5% settling time of 14ms.

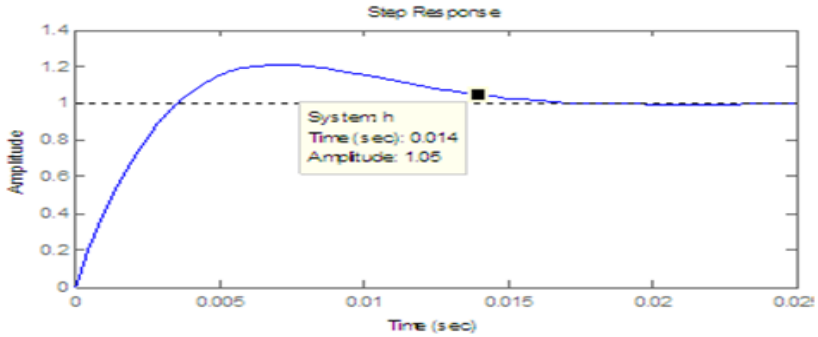

Fig. 15: Step response of the transfer function H(s).

Figure 16 shows the PLL behaviour in presence of an unbalanced voltage dips of type B and C. The PLL loop rejects the effect of these disturbances with a low ripple of angle θ_s.

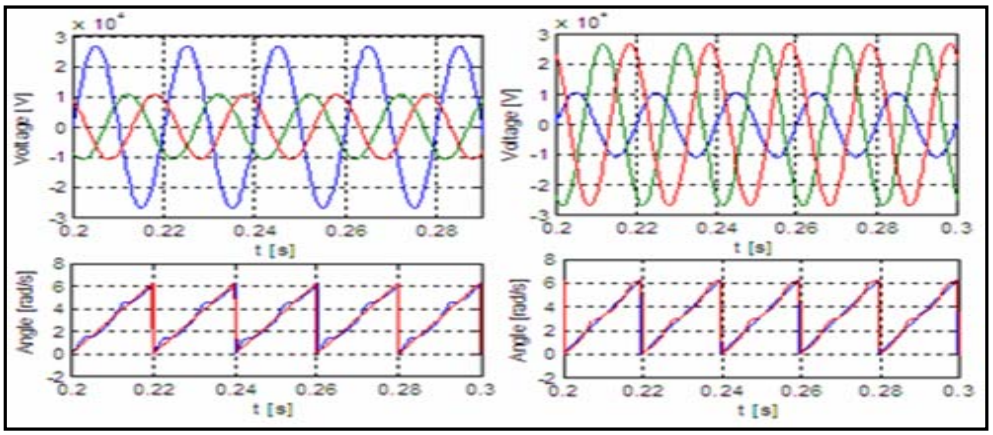

Fig. 16: Behaviour of the synchronization algorithm in the case of unbalanced voltage dips (Type B, C) with a 60% magnitude.

6. Wind system Performances

In this section, the wind system performances are analyzed and evaluated in term of accordance with the GCR of the German TSO, E. ON NEtz. Different case studies were performed. The system response was analyzed taking into consideration the normal operation mode, and the degraded operation mode.

6.1. Behaviour on normal operation

The following figures show the system behaviour in normal operation mode when the wind turbine produces its full rated power (2MW). It is noticed that active and reactive powers follow accurately their references. The DC-link voltage follows its reference and the voltage ripple does not exceed 2.5% of the nominal value.

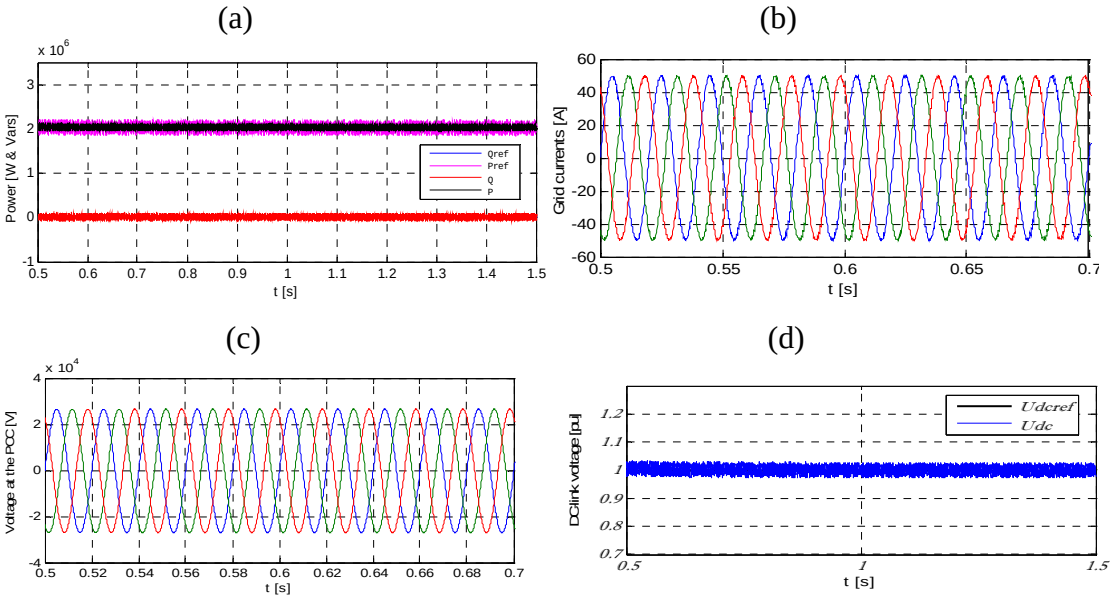

Fig. 17: Grid side converter response on normal operation. a) Reference power Pref & Qref and Produced power PQ. b) Grid current. c) Voltage at the PCC. d) DC-link voltage.

6.2. Power Quality

According to the IEEE 519 standards, the limit of harmonic distortions for distributed power systems connected to the grid should not exceed 5%. Figure 18 shows the harmonic content of grid currents at the PCC. This spectrum shows that the total harmonic distortion is 2.69% for current and 0.17% for the voltage. These results are in accordance with the IEEE 519 standard [11].

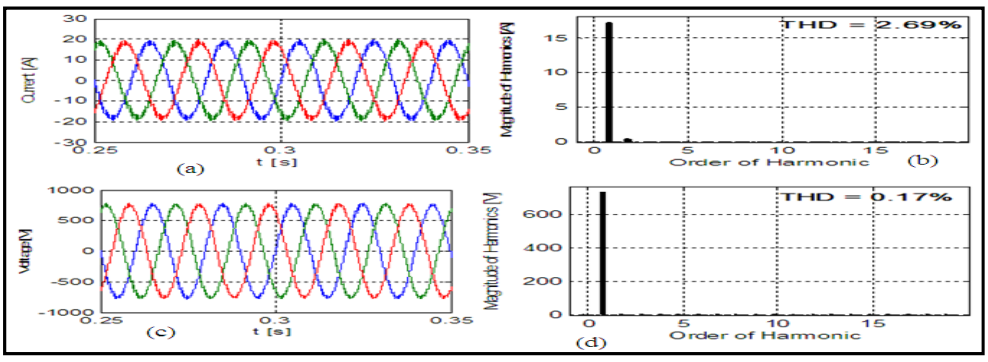

Fig. 18: a),c) Grid current and voltage. b), d) Grid current and voltage spectrum analysis.

6.3. Fault Ride Through Capability and support of grid voltage

Grid code of most countries requires that wind generators should stay connected to the grid in the case of grid faults. This is of particular importance to the TSOs, since wind farms tripping could lead to a major loss of power generation and consequently, power

system instability [12], [13]. The voltage profile of Figure 19 was applied in the PCC. This profile is defined by the TSO E.ON Netz for synchronous machines connected to the grid.

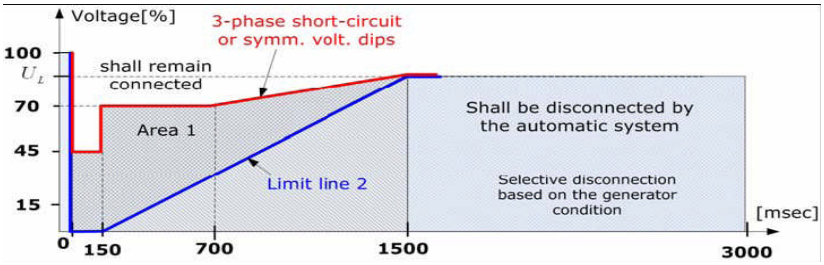

Fig. 19: Voltage profile according to the requirements of LVRT capability of synchronous generators according to [13].

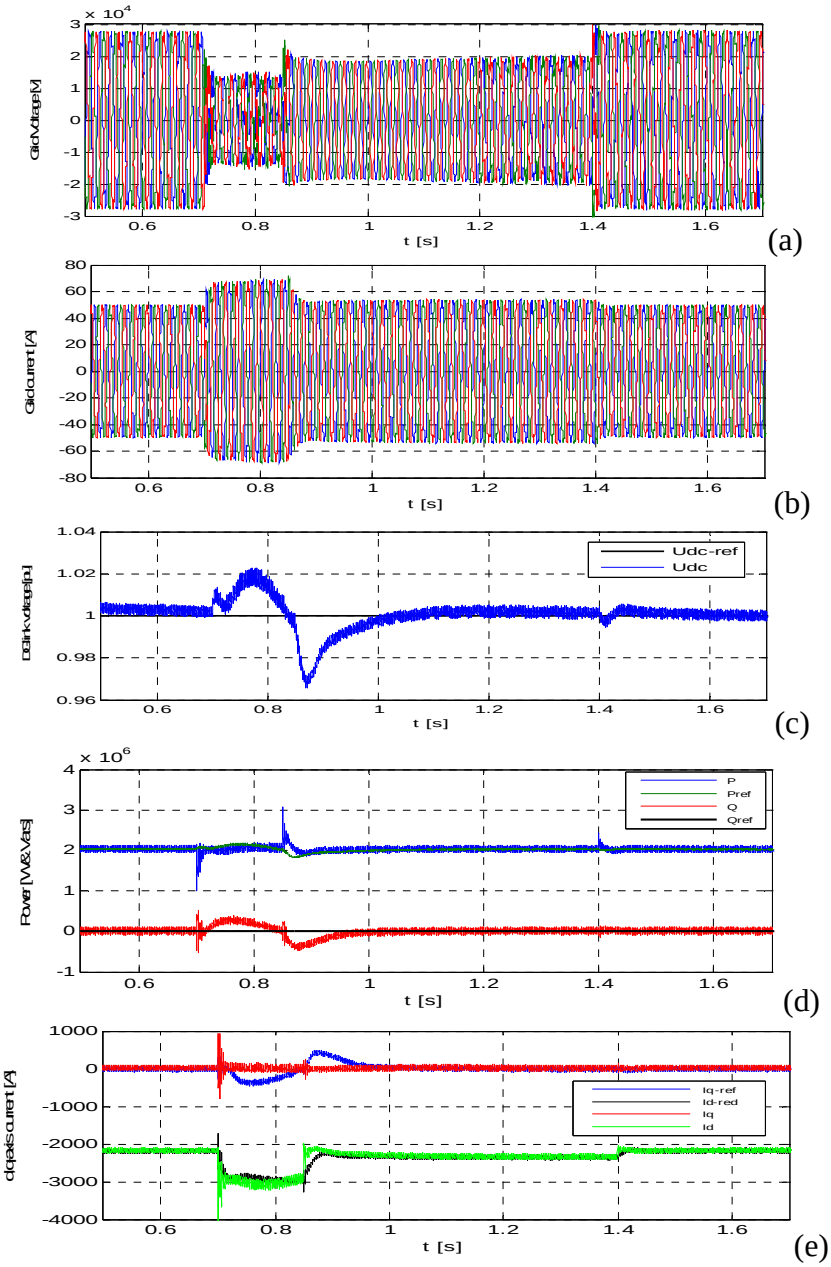

Fig. 20: a) Voltage at the PCC. b) Grid currents. c) DC-link voltage. d) Active and reactive powers. e) Reference and measured dq currents.

Figure 20 shows the wind system response in the case of the above mentioned voltage dip. Figure 20.a. and Figure 20.b. shows the voltage on the PCC and the grid currents. It can be observed that when the grid voltage increases, the grid currents decrease. This can be explained by the fact that the power flowing to the grid is constant (Fig. 20.d).

In Figure 20.c. the dc-link voltage is shown. The ripple of the DC-link voltage is a natural consequence of active power fluctuation. In Figure 20.e. the dq-currents are shown. Variations in the dq-reference currents allow bringing back the power and voltage to the desired values.

6.4. Frequency excursion

Grid frequency is an indicator of balance between the power production and consumption [14]. System operation is considered as safe when the frequency value is between 47.5 and 51.5 Hz and the voltage is between 80% and a bit above 100% [5, 12] of the rated value. For example, between 49.5 and 50.5 Hz, E.ON Netz requires the wind system to have the capability to operate continuously at normal rated output. If in some moment the frequency goes out of the predefined range, the wind turbine will be disconnected from the grid after the time fixed by the GCR [15]. In this section, the response of the wind system will be analysed in the case of grid frequency variation, by keeping the active power at 1 MW and the reactive power to zero. Grid frequency is chosen 0.5 Hz lower than its rated value. Figure 21.a. and Figure 21.b. show the voltage of the PCC and the grid currents. It can be observed that during the simulation the voltage of PCC has a fluctuation which produces transients in the grid currents. Figure 21.c. shows the dc-link voltage response. It can be noticed that voltage fluctuations are negligible compared to the rated value. Figure 21.d shows the active and reactive powers. It can be noticed that the wind system is insensitive to grid frequency variation.

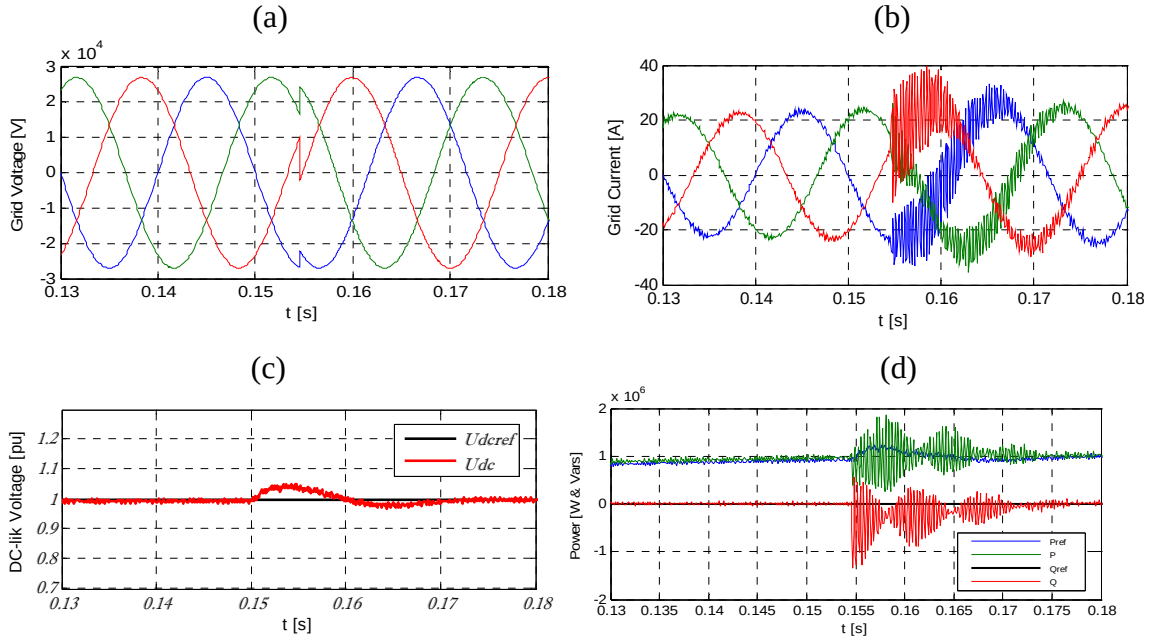

Fig. 21: a) Grid voltage. b) Grid current. c) DC-link voltage. d) Active and reactive power.

6.5. Response on degraded mode operation

Wind system connection to the grid must respect constraints on the frequency, amplitude and the phase of the voltage and should not affect the stability of the grid [16]. Thus the

disturbances produced at the PCC must be limited with regard to voltage dips, harmonics, imbalances... [17-18]. Figure 22 represents the simulation results obtained in the case of the degradation of the active power following a voltage dips of the type B of depth 50% (short-circuit occurs in one of the phases, (Figure (22.a)). Figures (22.b) and (22.c) show that the DC link voltage and active and reactive powers remain stable and follow their references in the case of grid fault. When the grid fault occurs the dc-link voltage decreases slightly and then reaches the reference value. Finally, it can be noticed that the wind turbine with direct drive offers another degree of freedom by keeping its stability during degradation of power and it complies with the grid connection requirement (G.C.R).

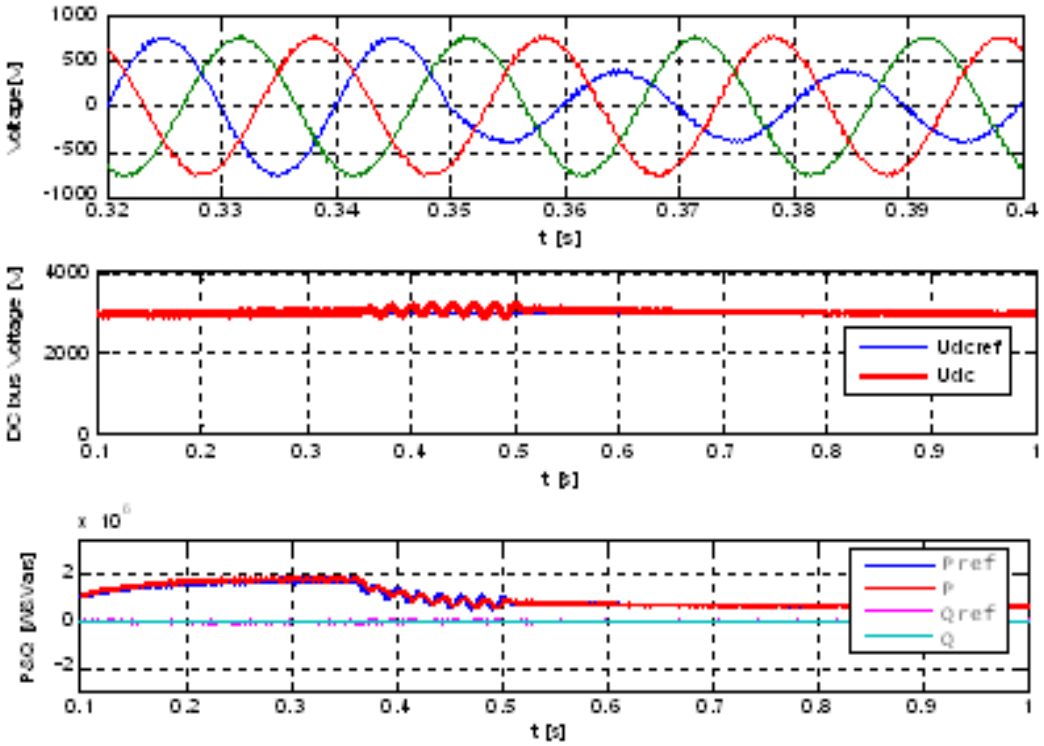

Fig. 22: a) Grid voltages. b) DC-link voltage. c) Active and reactive power.

7. Conclusion

During this work, The performances of the designed control strategy for the PMSG connected to the grid through a full scale back-to-back power converter has been assessed and illustrated by means of simulations for different operating conditions (up and down steps in low and large wind speeds). Direct drive wind turbine proved its aptitude to overcome the transient voltage faults and it can stay connected to the grid in the presence of the grid faults. In addition, the designed control strategy can be coupled to an external loop, ensuring energy supervision. In this way, it is possible to manage the wind park and ensure its stability during disturbances.

8. Acknowledgements

This work was supported by the Tunisian Ministry of High Education, Research and Technology.

9. REFERENCES

[1] C.F. Moyano and J.A. Pecas Lopes, An optimization approach for wind turbine commitment and dispatch in a wind park, Electric Power Systems Research, 79(1), 71–79, 2009.
[2] Y. Amirat, M. E. H. Benbouzid, B. Bensaker and R. Wamkeue. Generators for Wind Energy Conversion Systems: State of the Art and Coming Attractions, Journal of Electrical Systems, 3(1), 26-38, 2007.

[3] R. Pena, J.C. Clare and G.M. Asher, Doubly-fed induction generator using back-to-back PWM converters and its application to variable speed wind energy generation, IEEE proceedings on electronic power application, 143(3), 231-241, 1996.

[4] V. Akhmatov, Modelling and Ride-through Capabilities of Variable Speed Wind Turbines With Permanent Magnet Generators, Wiley Interscience, Vol 1, pp1-14 ,2005.

[5] S. Heier, Grid integration of wind energy conversion systems, Chichester: John Wiley & Sons Ltd, pp.35-302, 1998.
[6] S. Nouali and A. Ouali, Modelling and Control Strategy of a Wind Energy Conversion System based on a Doubly-Fed Twin Stator Induction Generator, Journal of Electrical Systems, 7(3), 343-357, 2011.

[7] H. Polinder, Overview and trends in wind turbine generator systems, IEEE Power and Energy Society General Meeting, 1-8, 2011.
[8] H. Geng, G. Yang, D. Xu and B. Wu, Unified Power Control for PMSG-Based WECS Operating Under Different Grid Conditions, IEEE Trans. on Energy Conversion, 26(3), pp. 822-830, 2011.

[9] S. Heier, Grid integration of wind energy conversion systems, John Wiley & Sons Ltd, 2nd ed.,Chichester, UK, 2006.
[10] F. Espin, E. Figueres and G. Garcera, An adaptive synchronous-reference-frame phase-locked loop for power quality improvement in polluted utility grid, IEEE Transactions on Industrial Electronics, 59(6), 2718-2731, 2012.

[11] IEEE STD 519-1992, IEEE Recommended Practices and Requirements for Harmonic Control in Electrical Power Systems, IEEE 519 working Group, 1992.

[12] E.ON Netz GmbH, Netzanschlussregeln für Hoch- und Höchstspannung, April 2006.

[13] F. Lov, A. Daniela Hansen, P. Sørensen and N. Antonio Cutululis, Mapping of grid faults and grid codes, Technical University of Denmark, VOL: Risø-R-1617(EN), Publisher: Risø National Laboratory, Roskilde Denmark, July 2007.

[14] M.G. Molina and P.E. Mercado, A new control strategy of variable speed wind turbine generator for three-phase grid-connected applications, Transmission and Distribution Conference and Exposition: Latin America, IEEE/PES, 1-8, Aug. 2008

[15] L.M. Fernandez, C.A. Garcia and F. Jurado, Operating capability as a PQ/PV node of a direct-drive wind turbine based on a permanent magnet synchronous generator, Renewable Energy, vol. 35, pp. 1308- 1318, 2010.
[16] F. Wu, X. P. Zhang and P. Ju, Small signal stability analysis and control of the wind turbine with the direct-drive permanent magnet generator integrated to the grid, Electric Power Systems Research, vol. 79, pp. 1661-1667, 2009.

[17] M. García-García, M. Paz Comech, J. Sallán, A. Llombart, Modelling wind farms for grid disturbance studies, Renewable Energy, vol. 33, 2109-2021, 2008.

[18] A. Abedini and A. Nasiri, Pmsg wind turbine performance analysis during short circuit faults, IEEE Canada Electrical Power Conference, pp. 160–165, 2007.

[19] G. Tapia, A. Tapia, J.X. Ostolaza, Two alternative modeling approaches for the evaluation of wind farm active and reactive power performances, IEEE Trans. Energy Convers. 21(4), 909–920, 2006.
[20] M.A. Abdullah, A.H.M. Yatim, C.W. Tan and R. Saidur, A review of maximum power point tracking algorithms for wind energy systems, Renew. Sustain, Energy Rev, 16, 3220–3227, 2012.

[21] H. Woo Kim, Sung-Soo Kim, Hee-Sang Ko, Modeling and control of PMSG-based variable-speed wind turbine, Electric Power Systems Research, vol. 80, 46-52, 2010.

[22] A. Kusiak and A. Verma , A data-driven approach for monitoring blade pitch faults in wind turbines, IEEE Trans. Sustainable Energy, 2(1), 87 -96, 2011.